Thermodynamics of the ideal overlap quarks on the lattice

Debasish Banerjee,[*] R. V. Gavai,[+] and Sayantan Sharma[‡]

Department of Theoretical Physics, Tata Institute of Fundamental Research, Homi Bhabha Road, Mumbai 400005, India

(Received 3 April 2008; revised manuscript received 14 June 2008; published 18 July 2008)

The thermodynamics of massless ideal gas of overlap quarks has been investigated both analytically and numerically for both zero and nonzero baryon chemical potential. Any μ^2 divergence is shown analytically to be absent for a class of actions with nonzero chemical potential. All such actions are shown to violate chiral invariance. While the parameter M can be shown to be irrelevant in the continuum limit, as expected, it is shown numerically that the continuum limit can be reached with relatively coarser lattices for $1.5 \leq M \leq 1.6$. Numerical limitations of the existing method of introduction of chemical potential are demonstrated. Finally we also show that the energy density for the massive overlap fermions has the correct continuum limit.

DOI: 10.1103/PhysRevD.78.014506 PACS numbers: 11.15.Ha, 12.38.Gc, 12.38.Mh

I. INTRODUCTION

Lattice QCD has so far provided the most reliable theoretical predictions for the thermodynamics of quarks and gluons important for the ongoing experiments at the Relativistic Heavy Ion Collider (RHIC), and may continue to do so for those at the upcoming Large Hadron Collider (LHC). While the equation of state seems [1] to exhibit robust features as one changes the number of light quarks N_f, the order of the phase transition and the transition temperature T_c seems [2] to depend on it crucially. Indeed, the location and even the existence of the critical point in the $\mu_B - T$ phase diagram is expected [3] to depend on N_f, as a result of this dependence of the order of the transitions on N_f. Since the transition seems to be associated with the restoration of the spontaneously broken chiral symmetry at high temperatures, it is very important to study it using fermions having exact chiral symmetries on the lattice. The popular choices of the fermions employed in simulations so far have either no chiral symmetry (Wilson fermions) on the lattice or only partial chiral symmetry (staggered fermions). For the latter even N_f is not well-defined on the lattice and is typically taken to be the anticipated continuum value. Of course, these issues are expected to become irrelevant in the continuum limit of vanishing lattice spacing, i.e, in the limit when the number of sites in the temporal direction becomes very large: $N_T \rightarrow \infty$. But they are likely to affect the current bunch of results obtained on lattices up to $N_T = 8$.

In view of the experimental relevance of these issues, it would clearly be ideal to employ fermions with exact chiral symmetry on lattice for investigations of the QCD thermodynamics. As is well-known by now, the overlap fermions [4] have such good chiral properties even on the lattice. The corresponding fermion operator respects chiral symmetry at the expense of being highly nonlocal, making the corresponding computations rather expensive. Advances in both algorithms and the computer hardware may have brought such investigations closer to reality today. In this paper we investigate the thermodynamics of the free overlap fermions with an aim to examine its continuum limit both analytically and numerically. For the above mentioned practical reasons, we investigate numerically whether the irrelevant parameter M (see below for explicit definition) can be tuned optimally to recover the continuum results on the smallest possible lattice size. These predictions can be used in full QCD simulations with such fermions to do the finite temperature calculations faster. A way to introduction of chemical potential in the overlap formalism was proposed [5] and has been recently studied [6] numerically with $M = 1$. It was shown that the known canonical μ^2 divergence at zero temperature did not appear. Our analytical work shows the absence of the divergence for all allowed M, $0 < M < 2$, for the same class [7] of actions as the staggered fermions.

The plan of our paper is as follows. Section II deals with zero chemical potential case. The analytical ($N_T \rightarrow \infty$) results for the energy density (equivalently pressure) at nonzero temperatures are derived and the numerical result for finite N_T are presented. Corresponding results for nonzero chemical potential are given in the next section, where the quark number susceptibility is also presented in addition. Section IV covers the case of massive quarks. A summary is provided in the final Sec. V.

II. ZERO CHEMICAL POTENTIAL

The overlap Dirac operator [4] has the following form for massless fermions on asymmetric lattice with spacing a and a_4 in the spatial and temporal directions:

$$D_{\mathrm{ov}} = 1 + \gamma_5 \mathrm{sgn}(\gamma_5 D_W), \tag{1}$$

where sgn denotes the signum function and

[*]debasish@theory.tifr.res.in
[+]gavai@tifr.res.in
[‡]ssharma@theory.tifr.res.in

$$D_W(x,y) = \left(3 + \frac{a}{a_4} - M\right)\delta_{x,y} - \frac{a}{a_4}\left[U_4^\dagger(x-\hat{4})\delta_{x-\hat{4},y}\frac{1+\gamma_4}{2} + \frac{1-\gamma_4}{2}U_4(x)\delta_{x+\hat{4},y}\right] - \sum_{i=1}^{3}\left[U_i^\dagger(x-\hat{i})\delta_{x-\hat{i},y}\frac{1+\gamma_i}{2} + \frac{1-\gamma_i}{2}U_i(x)\delta_{x+\hat{i},y}\right] \quad (2)$$

is the standard Wilson-Dirac operator on the lattice but with a negative mass term $M \in (0, 2)$. The overlap operator satisfies the Ginsparg-Wilson relation [8] and has exact chiral symmetry on the lattice. The corresponding infinitesimal chiral transformations [9] for $N_f = 1$ are

$$\delta\psi = \alpha\gamma_5\left(1 - \frac{1}{2}D_{\rm ov}\right)\psi \quad \text{and} \qquad \delta\bar{\psi} = \alpha\bar{\psi}\left(1 - \frac{1}{2}D_{\rm ov}\right)\gamma_5, \quad (3)$$

ψ and $\bar{\psi}$ are the usual four-component fermion and antifermion fields. They acquire a flavor index for higher N_f, with corresponding modification in the transformations above similar to that in the continuum. The expression for energy density and pressure can be obtained from the partition function $Z = \det D_{\rm ov}$ obtained by integrating the quark-antiquark fields

$$\epsilon = \frac{T^2}{V}\frac{\partial \ln Z(V,T)}{\partial T}\bigg|_V, \quad \text{and} \quad P = T\frac{\partial \ln Z(V,T)}{\partial V}\bigg|_T, \quad (4)$$

where the spatial volume $V = N^3a^3$ and the temperature $T = (N_T a_4)^{-1}$ for an $N^3 \times N_T$ lattice. We restrict ourselves to $U = 1$ here to focus on the ideal gas limit. Noting that the signum function for a matrix is defined in terms of its eigenvalues, the energy density can be written as

$$\epsilon = -\frac{1}{N^3a^3N_T}\left(\frac{\partial \ln(\prod_n \lambda_n)}{\partial a_4}\right)_a = -\frac{2}{N^3a^3N_T}\sum_{\lambda_\pm}\left(\frac{\partial \ln\lambda_\pm}{\partial a_4}\right)_a, \quad (5)$$

where the chiral nature of the eigenvalue spectrum in the free case was used. The eigenvalues of the free overlap operator in the momentum space can be easily worked [6,10] out to be

$$\lambda_\pm = 1 - \frac{\mathrm{sgn}(\sqrt{h^2 + h_5^2})h_5 \pm i\sqrt{h^2}}{\sqrt{h^2 + h_5^2}}, \quad (6)$$

where the variables h above are given by

$$h_5 = M - \sum_{j=1}^{3}(1 - \cos(ap_j)) - \frac{a}{a_4}(1 - \cos(a_4p_4)), \qquad h_j = -\sin(ap_j) \quad \text{where } j = 1,2,3, \qquad h_4 = -\frac{a}{a_4}\sin(a_4p_4), \qquad h^2 = h_1^2 + h_2^2 + h_3^2 + h_4^2. \quad (7)$$

From the (anti)periodic fermion boundary conditions in the (time) space directions, the discrete p_μ's appearing in the equations above are seen to have the following allowed values:

$$ap_j = \frac{2n_j\pi}{N}, \qquad n_j = 0,\ldots,(N-1), \qquad j = 1,2,3 \quad \text{and} \quad ap_4 = \frac{(2n+1)\pi}{N_T}, \qquad n = 0,\ldots,(N_T-1). \quad (8)$$

Note that the variables h_i are all real. Further, a simple algebra shows that $(h^2 + h_5^2) > 0$ for all ranges of interest for M, a, and a_4. Since the signum term in Eq. (6) is thus a constant, it does not contribute to the derivative in Eq. (5); it merely provides the overall sign for the energy density. Choosing $\mathrm{sgn}(\sqrt{h^2 + h_5^2}) = 1$, the energy density becomes

$$\epsilon = \frac{2}{N^3a^3N_T}\sum_{p_j,p_4}\frac{\frac{\partial h_5}{\partial a_4} - \frac{h_5}{h^2+h_5^2}(h_4\frac{\partial h_4}{\partial a_4} + h_5\frac{\partial h_5}{\partial a_4})}{\sqrt{h^2 + h_5^2} - h_5} = \frac{2}{N^3a^3N_T}\sum_{p_j,p_4}\frac{h^2\frac{\partial h_5}{\partial a_4} - h_5h_4\frac{\partial h_4}{\partial a_4}}{h^2(h^2+h_5^2)}(\sqrt{h^2+h_5^2} + h_5), \quad (9)$$

where the summations are over all the discrete sets of momenta on the lattice. The derivatives in the expression above are seen to be

$$\frac{\partial h_4}{\partial a_4} = -\frac{h_4}{a_4} \quad (10)$$

$$\frac{\partial h_5}{\partial a_4} = \frac{a}{a_4^2}(1 - \cos(a_4p_4)). \quad (11)$$

Similarly pressure P can be computed by taking partial derivative with respect to a, holding a_4 constant to obtain

$$P = \frac{-2}{3N^3a^2a_4N_T}\sum_{p_j,p_4}\frac{h^2\frac{\partial h_5}{\partial a} - h_5h_4\frac{\partial h_4}{\partial a}}{h^2(h^2+h_5^2)}(\sqrt{h^2+h_5^2} + h_5). \quad (12)$$

The derivatives in the expression for pressure are

$$\frac{\partial h_4}{\partial a} = \frac{h_4}{a} \tag{13}$$

$$\frac{\partial h_5}{\partial a} = -\frac{1}{a_4}(1 - \cos(a_4 p_4)). \tag{14}$$

Substituting the derivatives in Eqs. (9) and (12), one finds the expected ideal gas equation of state $\epsilon = 3P$, valid for all values of a and a_4. We shall therefore focus in the remainder only on the energy density for free overlap quarks on the lattice and evaluate it by setting $a_4 = a$. We introduce a more compact notation for doing so:

$$\begin{aligned} h_5 = g + \cos\omega \qquad h^2 = f + \sin^2\omega \\ h^2 + h_5^2 = d + 2g\cos\omega, \end{aligned} \tag{15}$$

where $\omega = ap_4$ and the functions g, f, and d are given by

$$\begin{aligned} g &= M - 4 + b, \quad \text{with} \\ b &= \cos(ap_1) + \cos(ap_2) + \cos(ap_3) \\ f &= h_1^2 + h_2^2 + h_3^2 \\ d &= 4 + (M-4)^2 + 2(M-4)b + c, \quad \text{with} \\ c &= \sum_{i<j<4} 2\cos(ap_i)\cos(ap_j). \end{aligned} \tag{16}$$

It may be noted that the g, d, and f depend only on spatial momenta p_j and enable us to write down the $ap_4 = \omega$ dependence of the energy density explicitly:

$$\begin{aligned} \epsilon a^4 = \frac{2}{N^3 N_T} \sum_{p_j,n} [(g + \cos\omega_n) + \sqrt{d + 2g\cos\omega_n}] \\ \times \Bigg[\frac{(1 - \cos\omega_n)}{d + 2g\cos\omega_n} \\ + \frac{\sin^2\omega_n (g + \cos\omega_n)}{(d + 2g\cos\omega_n)(f + \sin^2\omega_n)} \Bigg]. \end{aligned} \tag{17}$$

As shown in Appendix A, the summation over the Matsubara frequencies can be carried out using the standard contour integral techniques, resulting in the energy density on the lattice to be,

$$\epsilon a^4 = \frac{4}{N^3} \sum_{p_j} \left[\frac{\sqrt{f}}{\sqrt{1+f}} \right] \frac{1}{e^{N_T \sinh^{-1}\sqrt{f}} + 1} + \epsilon_3 + \epsilon_4, \tag{18}$$

where the ϵ_3, ϵ_4 terms come from the line integrals 3 and 4 in Fig. 8 respectively. Their explicit N_T dependence indicates that they contribute to the energy density on the lattice. However, they do not do so in the continuum limit, as we shall see below.

In order to take the continuum limit of $a \to 0$, we let N, $N_T \to \infty$ such that T and VT^3 are kept constant. Each summation over momenta is replaced by an integral in this limit:

$$\frac{1}{N} \sum_{p_j} \to \frac{a}{2\pi} \int_{-\infty}^{\infty} dp_j. \tag{19}$$

Further the integration variable $\omega = ap_4$ can be traded for p_4, pushing the branch points at $\pm\pi \pm i\cosh^{-1}\frac{d}{2g}$ to infinity faster than the contours 3 and 4 are pushed. The line integrals and hence the terms ϵ_3 and ϵ_4 vanish. Since the poles at $i\sinh^{-1}\sqrt{f}$ scale as a in this limit, they continue to be enclosed in the contour at a finite p_4 and do contribute to the energy density. This can, of course, be explicitly checked algebraically by taking the limit of Eq. (18) to obtain the expression for the continuum energy density as

$$\epsilon_{\rm SB} = \frac{2}{(2\pi)^3} \left(2 \int \prod_{j=1}^{3} dp_j \frac{E}{1 + e^{E/T}} \right) = \frac{7\pi^2}{60} T^4, \tag{20}$$

where $E = \sqrt{p_1^2 + p_2^2 + p_3^2}$ is the energy of the massless quarks.

A. Numerical evaluation

In this subsection we investigate the lattice energy density of Eq. (17) numerically by summing over all the momenta. Our aim is (i) to estimate the importance of the terms ϵ_3 and ϵ_4 in it on lattices of practical sizes, and (ii) to find out the role M plays on finite lattices. In particular, it would be good to know if there exists a range of the irrelevant parameter M for which the energy density converges to that of the continuum ideal Fermi gas on reasonable, i.e. computationally inexpensive, lattice sizes. Since we have shown the existence of the continuum limit for the entire allowed range of M in the previous subsection, it is clear that a sufficiently fine lattice must eventually yield the correct result for any M.

In general, the dimensionless lattice energy density will be of the form

$$E = A(M) + \frac{B}{N_T^4} + \frac{C(M)}{N_T^6} + \frac{D(M)}{N_T^8} + \cdots, \tag{21}$$

where the coefficients $A(M)$ and B are the usual vacuum and the T^4 contributions, while $C(M)$ and $D(M)$ are finite lattice spacing artifacts. For each value of M and aspect ratio, defined as $\zeta = N/N_T$, the energy density on the lattice was calculated as a function of the N_T. Clearly A is the dominant contribution and its removal turned out to be a tricky issue governed by the precision of our computations. Fitting the above form to obtain C or D was therefore not feasible. The zero temperature part of the energy density was calculated from Eq. (17) by taking $N_T \to \infty$ and a large spatial extent, keeping the lattice spacing finite. The resulting integral over ω was done numerically for each M to estimate the zero temperature contribution. Subtracting the zero temperature part from the energy density and dividing the resultant ϵ by $\epsilon_{\rm SB}$ gives us a ratio which we employ for further studies. Figure 1

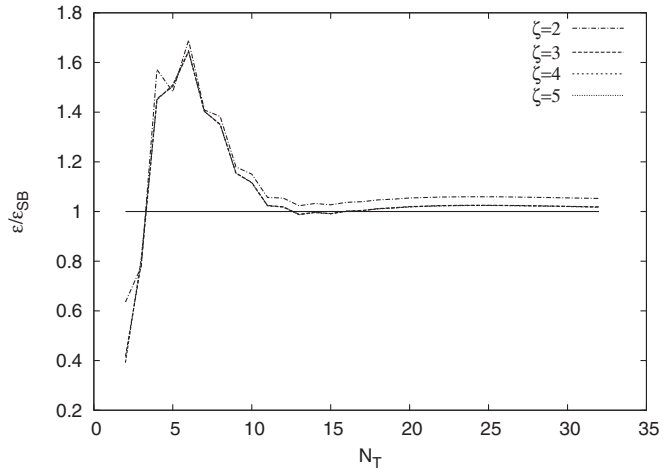

FIG. 1. The variation of the ratio $\epsilon/\epsilon_{\rm SB}$ with N_T for $M = 1.55$ and $\zeta = 2$–5.

displays the ratio $\epsilon/\epsilon_{\rm SB}$ as a function of N_T for $M = 1.55$ and various aspect ratios ζ. A mild dependence on ζ is visible for lower values but in each case the curve approaches to unity by $N_T = 12$, signalling the onset of continuum limit. Figure 2 exhibits the M dependence of the same ratio for a fixed $\zeta = 5$ for the range $0.4 \leq M \leq 1.65$. A range of $1.5 \leq M \leq 1.6$ emerges as the favored one because all the M-dependent terms are seen to be minimum there and hence the continuum limit is reached faster. On smaller lattices with $N_T = 4$–8, the lattice results are seen to be 1.6–1.8 times larger in this range of M. For other values of M, the continuum limit is seen to be approached slowly; even an $N_T = 25$ seems not enough. For larger M, we also observed oscillations as N_T changed between odd and even, limiting our effort to increase the M range further. The values of $\epsilon/\epsilon_{\rm SB}$ for $N_T = 4$–16 and different M are tabulated in Tables I and II, for easy reference. We note that the $\zeta = 3, 4$ results are the same

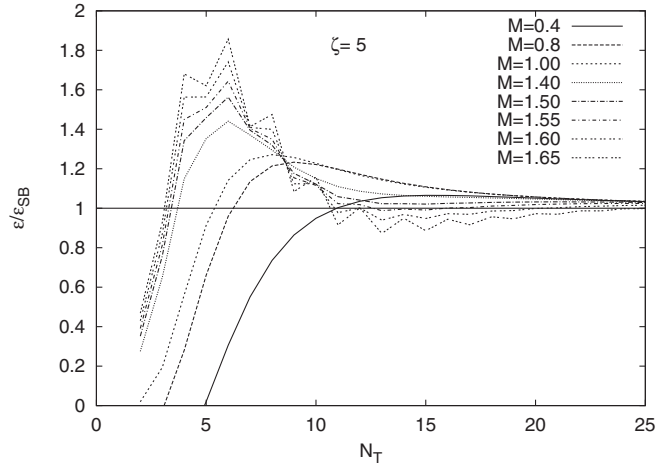

FIG. 2. The variation of the ratio $\epsilon/\epsilon_{\rm SB}$ with N_T for different M and $\zeta = 5$.

TABLE I. $\epsilon/\epsilon_{\rm SB}$ values for different M for $\zeta = 2$.

N_T	$M = 1.0$	1.50	1.55	1.60	1.65
4	0.630	1.453	1.571	1.697	1.828
6	1.194	1.606	1.690	1.792	1.914
8	1.316	1.355	1.383	1.431	1.506
10	1.268	1.158	1.150	1.156	1.186
12	1.206	1.078	1.054	1.036	1.033
14	1.160	1.060	1.032	1.004	0.983
16	1.129	1.061	1.037	1.008	0.979

TABLE II. $\epsilon/\epsilon_{\rm SB}$ values for different M for $\zeta = 5$.

N_T	$M = 1.0$	1.50	1.55	1.60	1.65
4	0.561	1.342	1.450	1.563	1.681
6	1.141	1.563	1.644	1.742	1.857
8	1.272	1.319	1.350	1.399	1.475
10	1.228	1.122	1.116	1.124	1.157
12	1.167	1.041	1.018	1.001	1.002
14	1.123	1.023	0.996	0.969	0.950
16	1.092	1.025	1.001	0.972	0.944

as that for $\zeta = 5$ as seen from Fig. 1. In order to estimate the size of the $1/N_T^2$ correction term for different values of M, the same ratio is plotted as a function of $1/N_T^2$ in Fig. 3. From the plot, it is evident that the correction terms die down very fast for $1.50 \leq M \leq 1.60$ and the continuum limit is reached within 2–3% already for $N_T = 12$ whereas for $M = 1$ they are relevant even for $N_T \geq 12$. Of course, the continuum extrapolation for $M = 1.0$ is easier than for $1.50 \leq M \leq 1.60$ due to the nonlinearities present for the latter. Note, however, that energy density for at least three different lattice sizes with $N_T = 10, 12, 14$ needs to be

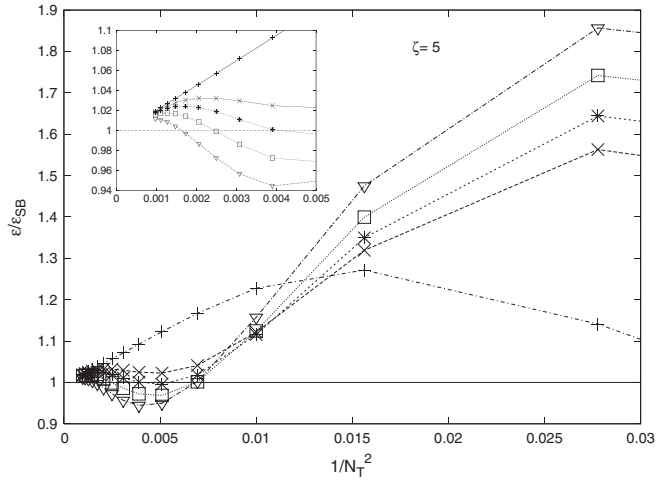

FIG. 3. The variation of the ratio $\epsilon/\epsilon_{\rm SB}$ with $1/N_T^2$ for different $M \geq 1$ and $\zeta = 5$. The plusses, crosses, stars, boxes, and triangles denote $M = 1.0$, 1.50, 1.55, 1.60 and 1.65, respectively.

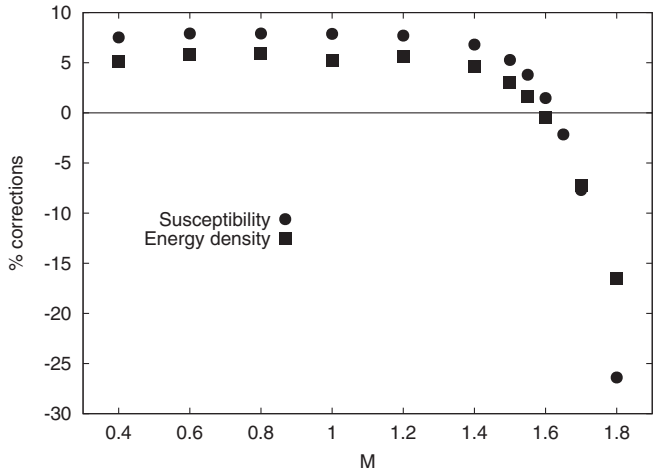

FIG. 4. The estimated finite lattice spacing corrections for the energy density and susceptibility at $\mu = 0$ in percentage as a function of M.

computed for such an extrapolation. On the other hand, although the extrapolation for $1.50 \leq M \leq 1.60$ is difficult due to the complex variation seen in Fig. 3, the deviation from the continuum value is within the typical accuracy range of the current lattice results, making it an optimal range for simulations. It should also be noted that the corrections for the overlap fermions for $M \sim 1.55$ for $N_T < 12$ are smaller than compared to the Wilson and the staggered case [11] as well. Reference [11] deals with p/p_{SB} which we showed above to be identical to the $\epsilon/\epsilon_{\mathrm{SB}}$ for the overlap ideal gas.

Filled squares in Fig. 4 show the percentage average deviations of the ratio from unity due to lattice artifact terms as a function of M for large N_T values ($N_T \geq 18$). It shows marginal dependence on M for $M < 1.2$ but the deviation itself is about 5–6%. For larger M, the data show a dip, indicating clearly that the thermodynamics of free fermions favors the optimum value of M to lie between 1.50–1.60, with a deviation of only about 2.5% or lower.

Comparing our results with other studies of thermodynamics of free fermions done with improved actions [12] and also with overlap fermions ($M = 1$) in 2D [13] as well as in 4D [6,11], we find that (i) there are larger deviations in higher dimensions and (ii) the oft-favored choice of $M = 1$ favors rather poorly on finite lattices. Indeed, one can significantly reduce the corrections to the energy density of overlap fermions due to the lattice artifacts with a proper choice of M.

III. NONZERO CHEMICAL POTENTIAL

The chemical potential is usually introduced as the Lagrange multiplier to investigate thermodynamics at constant conserved number. Constructing the relevant number operator for the overlap Dirac fermions is not easy due to its nonlocality [14] and may even be not unique [15]. Instead of deriving the conserved number, one may make an inspired guess for it such that it has the right continuum limit. One such proposal for introducing the chemical potential for the overlap operator is [5] to introduce it in the D_W as one would for the usual Wilson fermions:

$$D_{\mathrm{ov}} = 1 + \gamma_5 \mathrm{sgn}(\gamma_5 D_W(\hat{\mu})), \tag{22}$$

where the chemical potential $\hat{\mu} = \mu a_4$ appears only as multiplying factors $\exp(\hat{\mu})$ and $\exp(-\hat{\mu})$ to the links U_4 and $U_4^\dagger$ respectively in Eq. (2). This, of course, renders $\gamma_5 D_W(\mu)$ to be non-Hermitian, necessitating an extension of the usual definition of the signum function. The natural choice [5] was to use the sign of the real part of the eigenvalues of $\gamma_5 D_W(\mu)$ in the equation above. It is important to note that the extended signum function it is not defined for purely imaginary eigenvalues. Numerical simulations were performed [6] for an ideal gas of overlap fermions to show that the above way of introducing μ does not encounter any quadratic divergences at zero temperature. Such divergences were known to arise [16,17] for staggered and Wilson fermions, if μ was introduced naively as a coefficient of the conserved number. These were eliminated by the choice of the $\exp(\pm\hat{\mu})$ factors. A more general way to introduce the chemical potential is, of course, to introduce functions $K(\hat{\mu})$ and $L(\hat{\mu})$ in place of the factors $\exp(\hat{\mu})$ and $\exp(-\hat{\mu})$ respectively such that $K(\hat{\mu}) = 1 + \hat{\mu} + \mathcal{O}(\hat{\mu}^2)$ and $L(\hat{\mu}) = 1 - \hat{\mu} + \mathcal{O}(\hat{\mu}^2)$. It was shown [7] that the quadratic divergences are avoided if $K(\hat{\mu}) \cdot L(\hat{\mu}) = 1$.

Here we follow that idea and introduce chemical potential in the overlap Dirac operator through the K and L factors in D_W and study where the condition to eliminate the quadratic divergences remains the same. Introducing

$$\frac{K(\hat{\mu}) - L(\hat{\mu})}{2} = R\sinh\theta \qquad \frac{K(\hat{\mu}) + L(\hat{\mu})}{2} = R\cosh\theta, \tag{23}$$

one can follow through the steps of the previous section to find that the free overlap operator in the momentum space can again be written in terms of the h_i of Eq. (7) but with h_4 and h_5 changed to

$$h_5 = M - \sum_{j=1}^{3}(1 - \cos(ap_j)) - \frac{a}{a_4}(1 - R\cos(a_4 p_4 - i\theta))$$
$$h_4 = -\frac{a}{a_4} R\sin(a_4 p_4 - i\theta). \tag{24}$$

The energy density in presence of finite chemical potential is defined as

$$\epsilon(\mu) = -\frac{1}{N^3 a^3 N_T}\left(\frac{\partial \ln \det D}{\partial a_4}\right)_{a,a_4\mu} \tag{25}$$

$$= -\frac{2}{N^3 a^3 N_T}\left(\frac{\partial \ln(\lambda_+\lambda_-)}{\partial a_4}\right)_{a,a_4\mu}. \tag{26}$$

In the following we assume that the signum function is always defined and is $+1$, as for the $\mu = 0$ case. We shall comment on this assumption later. The energy density is obtained using Eq. (25) and setting $a = a_4$,

$$\epsilon a^4 = \frac{2}{N^3 N_T}\sum_{p_j,n}\Bigg[\frac{1 - R\cos(\omega_n - i\theta)}{d_R + 2gR\cos(\omega_n - i\theta)} + \frac{R^2\sin^2(\omega_n - i\theta)(g + R\cos(\omega_n - i\theta))}{(d_R + 2gR\cos(\omega_n - i\theta))(f + R^2\sin^2(\omega_n - i\theta))}\Bigg] \times [g + R\cos(\omega_n - i\theta) + \sqrt{d_R + 2gR\cos(\omega_n - i\theta)}]. \tag{27}$$

Note that the summand in the equation above has the same functional form as that in Eq. (17). Indeed the only changes are: $d_R = f + g^2 + R^2$ replaces d of Eq. (16), $\omega \to \omega - i\theta$, and the factor R multiplies each sine/cosine term. Let us therefore denote the summand in Eq. (27) as $F(R, \omega - i\theta)$. Comparing Eq. (24) with Eq. (7), and using the expression for the pressure given in Eq. (12), one again finds that the equation of state $\epsilon = 3P$ also holds in the presence of a chemical potential μ. An additional new physical observable that can be computed is the number density, defined as

$$n = \frac{1}{N^3 a^3 N_T}\left(\frac{\partial \ln \det D}{\partial \hat{\mu}}\right)_{a_4}. \tag{28}$$

In terms of h's the previous expression can be calculated explicitly,

$$na^3 = \frac{-2i}{N^3 N_T}\sum_{p_j,n}\Bigg[R\sin(\omega_n - i\theta)\left(\frac{gR\cos(\omega_n - i\theta) + R^2 + f}{(d_R + 2gR\cos(\omega_n - i\theta))(f + R^2\sin^2(\omega_n - i\theta))}\right) \times \left(g + R\cos(\omega_n - i\theta) + \sqrt{d_R + 2gR\cos(\omega_n - i\theta)}\right)\Bigg] = \frac{-2i}{N^3 N_T}\sum_{p_j,n} F_N(R, \omega_n - i\theta). \tag{29}$$

A. Analytic results

In order to obtain the condition for removing the divergences, we first calculate the energy density at zero temperature i.e for the limit $N_T \to \infty$ at finite a. The frequency sum $\frac{1}{N_T}\Sigma$ in Eq. (27) gets replaced by the integral $\frac{1}{2\pi} \times \int_{-\pi}^{\pi} d\omega$. Subtracting the vacuum contribution corresponding to $\mu = 0$, i.e., $R = 1$, $\theta = 0$, the energy density at zero temperature is given by

$$\epsilon a^4 = \frac{1}{\pi N^3}\sum_{p_j}\Bigg[\int_{-\pi}^{\pi} F(R, \omega - i\theta)d\omega - \int_{-\pi}^{\pi} F(\omega)d\omega\Bigg]. \tag{30}$$

Choosing the contour shown in Fig. 5, the expression above can be evaluated in the complex ω plane as

$$\epsilon a^4 = \frac{1}{\pi N^3}\sum_{p_j}\Bigg[2\pi i\sum_i \mathrm{Res}F(R, \omega_i) - \int_{\pi - i\theta}^{\pi} F(R, \omega)d\omega - \int_{\pi}^{-\pi} F(R, \omega)d\omega - \int_{-\pi}^{-\pi - i\theta} F(R, \omega)d\omega - \int_{-\pi}^{\pi} F(\omega)d\omega\Bigg]. \tag{31}$$

The second and fourth terms cancel since F is an even function which satisfies $F(\pi + i\eta) = F(-\pi + i\eta)$. Hence, we obtain

$$\epsilon a^4 = \frac{1}{\pi N^3}\sum_{p_j}\Bigg[2\pi R_3\Theta\left(\frac{K(\hat{\mu}) - L(\hat{\mu})}{2} - \sqrt{f}\right) + \int_{-\pi}^{\pi} F(R, \omega)d\omega - \int_{-\pi}^{\pi} F(\omega)d\omega\Bigg], \tag{32}$$

where $-iR_3$ is the residue of the function $F(R, \omega)$ at the pole $-i\sinh{-1}(\sqrt{f}/R)$ and is given by

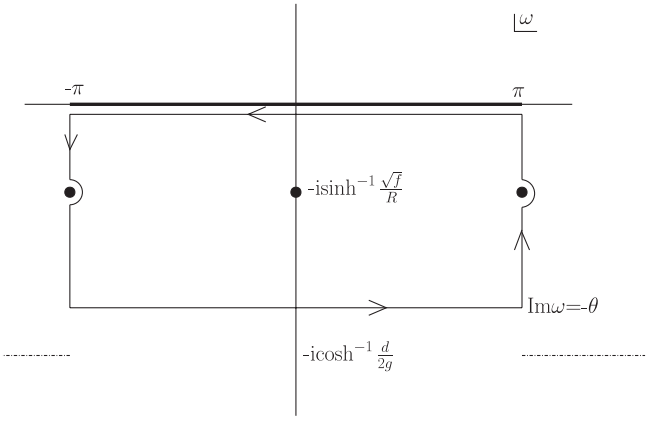

FIG. 5. Contour chosen for evaluating the energy density and the number density for nonzero of chemical potential at zero temperature. The thick line indicates the Matsubara frequencies while the filled circles denote the poles of $F(R, \omega)$.

$$R_3 = \frac{\sqrt{f}(g+\sqrt{f+R^2}+\sqrt{d_R+2g\sqrt{f+R^2}})}{2\sqrt{f+R^2}(d_R+2g\sqrt{f+R^2})}(g + \sqrt{f+R^2}). \quad (33)$$

Noting that the number density in Eq. (29) has the same pole structure as the energy density, with only the residues being different in the two cases, the latter can also be calculated in the same way to obtain

$$na^3 = \frac{1}{\pi N^3}\sum_{p_j}\Big[2\pi R_4\Theta\Big(\frac{K(\hat{\mu})-L(\hat{\mu})}{2}-\sqrt{f}\Big) - i\int_{-\pi}^{\pi}F_N(R,\omega)d\omega + i\int_{-\pi}^{\pi}F_N(\omega)d\omega\Big], \quad (34)$$

where R_4 is the residue of the function $F_N(\omega)$ at the pole $-i\sinh{-1}(\sqrt{f}/R)$ given by

$$R_4 = \frac{(g+\sqrt{f+R^2}+\sqrt{d_R+2g\sqrt{f+R^2}})}{2\sqrt{f+R^2}(d_R+2g\sqrt{f+R^2})} \times (g\sqrt{R^2+f}+R^2+f).$$

It is clear from both Eqs. (32) and (34) that the condition $R = 1$ cancels the two integrals in each of them, yielding the canonical forms of the Fermi surface. For $R \neq 1$, there will in general be violations of the Fermi surface on the lattice. Moreover, in the continuum limit $a \to 0$, one will in general have the μ^2/a^2 divergences for $R \neq 1$ in both the energy density and the number density. The condition to obtain the correct continuum values of $\epsilon = \mu^4/4\pi^2$ and $n = \mu^3/3\pi^2$ can also be seen to be the expected $K(\hat{\mu}) - L(\hat{\mu}) = 2\hat{\mu} + O(\hat{\mu}^2)$. Note that the earlier work [7] on staggered fermions employed the exact number density on the lattice which is not the case for the overlap fermions here. That one obtains still identical conditions in both the cases suggests that it is indeed the behavior near the continuum limit which dictates these conditions.

Another crucial difference is that the introduction of the functions K and L for the staggered fermions still leaves the action invariant under the chiral transformations due to the locality of the action. This is true for the full theory, i.e., even after the link variables U_x^μ are restored. On the contrary, one can easily check that one breaks the chiral invariance in the case of the overlap fermions by these functions K, L, or $\exp(\pm\hat{\mu})$. As defined in Eq. (3), the chiral transformation involves $D_{\rm ov}(\hat{\mu}=0)$, while the action for $\mu \neq 0$ for the overlap fermions has $D_{\rm ov}(\hat{\mu})$ of the Eq. (22). By construction, the latter does satisfy the Ginsparg-Wilson relation [8] with the μ-dependent overlap Dirac operator on both sides:

$$\{\gamma_5, D_{\rm ov}(\hat{\mu})\} = D_{\rm ov}(\hat{\mu})\gamma_5 D_{\rm ov}(\hat{\mu}). \quad (35)$$

Unfortunately though, it is not sufficient to guarantee invariance under the chiral transformation in Eq. (3), as it does not have any μ dependence. Indeed, the variation of action under the chiral transformation of Eq. (3) is

$$\delta S = \alpha\sum_{x,y}\bar{\psi}_x[\gamma_5 D_{\rm ov}(\hat{\mu}) + D_{\rm ov}(\hat{\mu})\gamma_5 - \frac{1}{2}D_{\rm ov}(0)\gamma_5 D_{\rm ov}(\hat{\mu}) - \frac{1}{2}D_{\rm ov}(\hat{\mu})\gamma_5 D_{\rm ov}(0)]_{xy}\psi_y, \quad (36)$$

which clearly does not vanish in spite of Eq. (35).

Finally, using the same techniques to evaluate the Matsubara frequencies sum, the energy density at nonzero temperature and chemical potential can be computed analytically. Further details are given in Appendix B. The final expression is

$$\epsilon a^4 = \frac{2}{N^3}\sum_{p_j}\Big[\frac{\sqrt{f}}{\sqrt{1+f}}\frac{1}{e^{(\sinh^{-1}\sqrt{f}-\hat{\mu})N_T}+1} + \frac{\sqrt{f}}{\sqrt{1+f}}\frac{1}{e^{(\sinh^{-1}\sqrt{f}+\hat{\mu})N_T}+1} + \epsilon_{3\mu} + \epsilon_{4\mu}\Big]. \quad (37)$$

The terms $\epsilon_{3\mu}$ and $\epsilon_{4\mu}$ are contributions of the line integrals in Figs. 9 and 10. They vanish in the continuum limit leaving only the contribution due to the residues of the poles shown in those figures. It can be shown explicitly that the expression for the lattice energy density reduces to the well-known [18] result in the continuum.

$$\epsilon = \frac{2}{(2\pi)^3}\int\frac{E\prod_{j=1}^3 dp_j}{1+e^{(E+\mu)/T}} + \frac{2}{(2\pi)^3}\int\frac{E\prod_{j=1}^3 dp_j}{1+e^{(E-\mu)/T}}. \quad (38)$$

B. Numerical evaluation

As in Sec. , our aim of presenting numerical results by carrying out the sums over all momenta in Eq. (B7) is to find out the importance of lattice artifacts in form of the terms involving $\epsilon_{3\mu}$ and $\epsilon_{4\mu}$, resulting from the line integrals 3 and 4, and to look for the role of M. The focus here is, of course, on the chemical potential. We therefore consider two observables here. One is the change in the energy density $\Delta\epsilon(\mu,T) = \epsilon(\mu,T) - \epsilon(0,T)$. In continuum it is given by

$$\frac{\Delta\epsilon(\mu,T)}{T^4} = \frac{\mu^4}{4\pi^2T^4} + \frac{\mu^2}{2T^2}. \quad (39)$$

The other quantity we consider is the quark number susceptibility at $\mu \hat{=} 0$. For the free overlap fermions, it is given for any $\hat{\mu}$ by

$$\chi = \frac{1}{N^3a^2N_T}\Big(\frac{\partial^2 \ln \det D}{\partial\hat{\mu}^2}\Big)_{a_4}, \quad (40)$$

which can be worked out to be

$$\chi = \frac{2i}{N_T N^3 a^2} \sum_{p_j, p_4} \left[\frac{-(h^2 h_4 + h_4 h_5 \cos(a p_4 - i\hat{\mu}))u}{s^4 (s - h_5)^2} + \frac{v}{s^2 (s - h_5)} \right]. \quad (41)$$

u and v are in the expression above are

$$u = 2(s - h_5)\left(h_4 \frac{\partial h_4}{\partial \hat{\mu}} + h_5 \frac{\partial h_5}{\partial \hat{\mu}} \right) + s^2 \left(\frac{\partial s}{\partial \hat{\mu}} - \frac{\partial h_5}{\partial \hat{\mu}} \right), \quad (42)$$

$$v = \frac{\partial h_4}{\partial \hat{\mu}} (2h_4^2 + h^2 + h_5 \cos(a p_4 - i\hat{\mu})) + h_4 \frac{\partial h_5}{\partial \hat{\mu}} \cos(a p_4 - i\hat{\mu}) + i h_4 h_5 \sin(a p_4 - i\hat{\mu}), \quad (43)$$

and

$$s^2 = h^2 + h_5^2. \quad (44)$$

Again in the continuum, the susceptibility is known to be

$$\chi(\mu) = \frac{\mu^2}{\pi^2} + \frac{T^2}{3}. \quad (45)$$

Our computations for the energy density were performed keeping the ratio $r = \mu/T = \hat{\mu} N_T$ fixed, yielding a constant $\Delta\epsilon/T^4$ in the continuum from Eq. (39). Our choices of r were restricted by the fact that on lattices with odd N_T, eigenvalues of $\gamma_5 D_W(\hat{\mu})$ can turn purely imaginary for sufficiently large $\hat{\mu}$. This is related to the fact that $(\gamma_5 D_W)^\dagger \gamma_5 D_W$ has $h^2 + h_5^2$ as eigenvalues and

$$\mathrm{Re}(h^2 + h_5^2) = g^2 + 1 + f + 2g \cos\omega \cosh\hat{\mu}$$
$$\mathrm{Im}(h^2 + h_5^2) = 2g \sin\omega \sinh\hat{\mu} \quad (46)$$

has zero imaginary part at $\omega = \pi$ with negative real part for $\mu \geq \mu_c$. The signum function is undefined for such cases. Indeed, in the interacting case it may even be possible to get such purely imaginary argument of the signum function of the overlap Dirac operator for all N_T.

From the plots of the ratio of the $\Delta\epsilon/T^4$ on the lattice and in the continuum [Eq. (39)] shown in Fig. 6, we again conclude that the continuum limit is reached for $N_T \geq 12$ for both the cases for essentially all M, with the $1.5 < M < 1.6$ region displaying the smallest deviations in the region $N_T > 12$ as in the $\mu \hat{=} 0$ case in Sec. . Moreover the results for $\Delta\epsilon$ again appear about 1.6–1.8 times larger on the

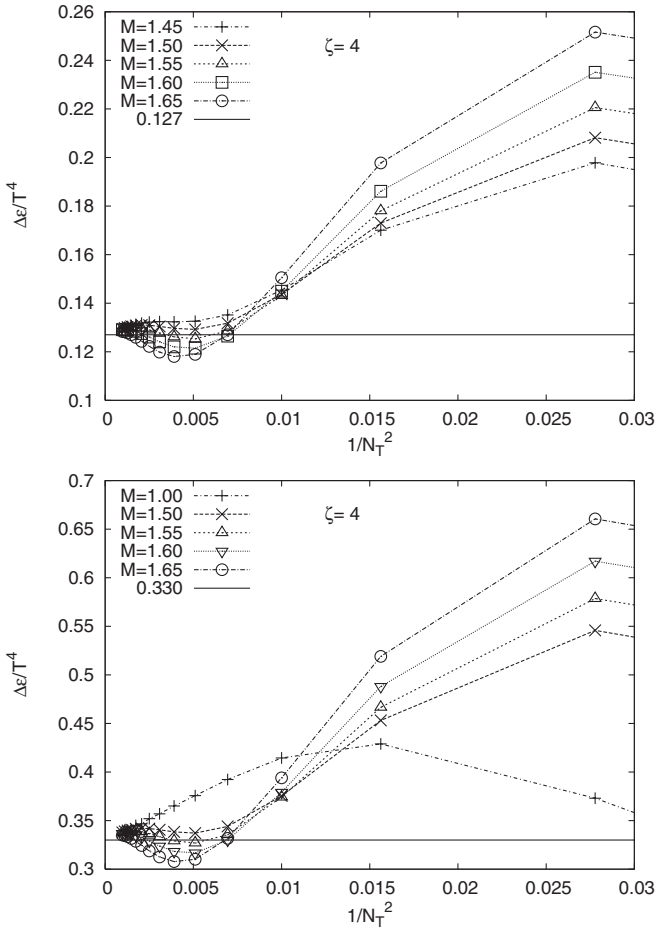

FIG. 6. The variation of the lattice $\Delta\epsilon/T^4$ with $1/N_T^2$ for $\hat{\mu} = 0.5/N_T$ (upper panel) and $\hat{\mu} = 0.8/N_T$ (lower panel).

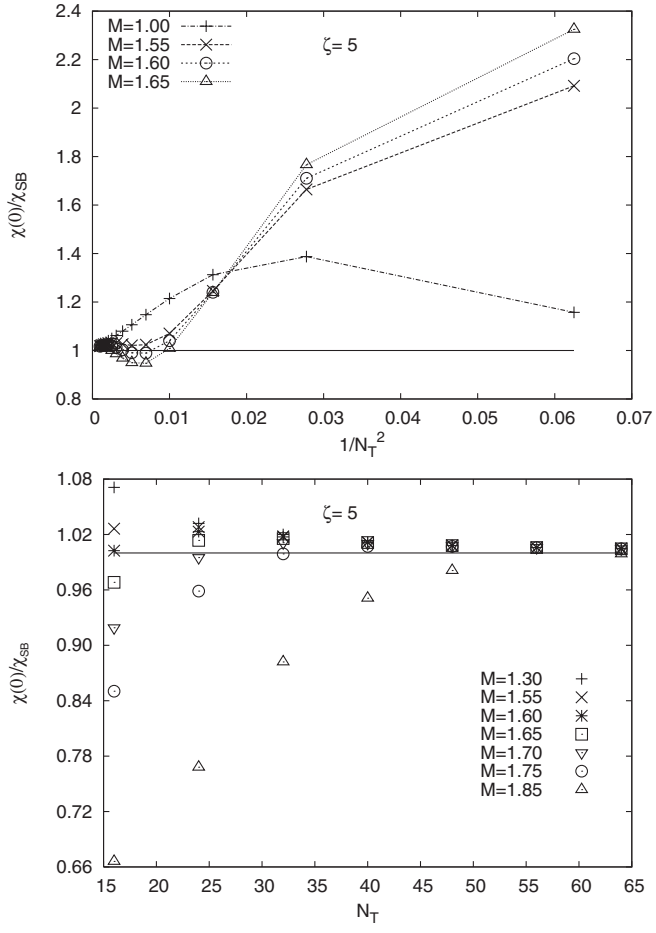

FIG. 7. The variation of $\chi(0)/\chi_{\mathrm{SB}}$ vs $1/N_T^2$ (upper panel) and vs N_T (lower panel) for different M and $\zeta = 5$.

lattices with $N_T = 4$–8 while the susceptibility is close to twice the continuum result.

In the upper panel of Fig. 7, we display the ratio of $\chi(\mu = 0, T)$ on the lattice with the corresponding continuum value from Eq. (45). One sees again a similar pattern as for the energy density. As in Eq. (21), the susceptibility calculated on the lattice will also have a form

$$\chi(0) = \frac{B^\chi}{N_T^2} + \frac{C^\chi(M)}{N_T^4} + \frac{D^\chi(M)}{N_T^6} + \cdots, \tag{47}$$

where the only difference is the absence above of a constant term like A. Keeping only the first term, one will again get the effective B^χ to become M dependent; its deviation from $1/3$ will be a measure of the finite lattice spacing effects. The filled circles in Fig. 4 display these artifact effects as a function of M which were obtained by assuming a constant behavior in the range $18 \leq N_T \leq 32$. The absence of a dominant term like A in the equation above allowed us to redo the fit with the inclusion of the next term for each M. We found that the resultant B^χ is already M independent and close to $1/3$ in each case. Moreover the C^χ changed with M substantially and was smallest for $M = 1.6$. From all these fits, it also emerged that by $N_T = 64$ the contribution of the C^χ term becomes negligible. The lower panel of Fig. 7 exhibits the results of our attempt to verify this by extending the computations to larger lattices. One does, indeed, find a convergence to the continuum result irrespective of the value of M from lattice sizes of $320^3 \times 64$. Note that one finds very similar effects of finite lattice spacing for both the susceptibility and the energy density at $\mu = 0$ in Fig. 4, with $M \sim 1.6$ emerging as a good choice for calculations on lattices with small N_T due to smallest values of the correction terms.

IV. MASSIVE OVERLAP FERMIONS

While we restricted ourselves to the thermodynamics of massless overlap fermions, most of our treatment goes through for the massive fermions as well. In this section we outline this for the $\mu = 0$ case. For the sake of novelty, we use an alternative way of doing the computation. The overlap operator for fermions of mass m is written as

$$D_{\rm ov} = \left(1 + \frac{m}{2M}\right) + \left(1 - \frac{m}{2M}\right)\gamma_5 \,\mathrm{sgn}(\gamma_5 D_W). \tag{48}$$

The eigenvalues of the overlap Dirac operator change from $\lambda_\pm$ in Eq. (6) to $\lambda_\pm \to \lambda_\pm(1 - m/2M) + m/M$. As a result the energy density modifies from Eq. (9) to

$$\epsilon = \frac{2}{N^3 a^3 N_T} \sum_{p_j, p_4} \frac{\alpha(h^2 \frac{\partial h_5}{\partial a_4} - h_5 h_4 \frac{\partial h_4}{\partial a_4})}{(h^2 + h_5^2)(\gamma\sqrt{h^2 + h_5^2} - \alpha h_5)}, \tag{49}$$

where

$$\alpha = 2\left(1 - \frac{m^2 a^2}{4M^2}\right) \quad \text{and} \quad \gamma = 2\left(1 + \frac{m^2 a^2}{4M^2}\right).$$

Substituting the values of h_4, h_5, and their derivatives, one obtains

$$\epsilon a^4 = \frac{2\alpha}{N^3 N_T} \sum_{p_j, n} \Bigg[\frac{(1 - \cos\omega_n)(f + \sin^2\omega_n)}{(d + 2g\cos\omega_n)(\gamma^2(d + 2g\cos\omega_n) - \alpha^2(g + \cos\omega_n)^2)} + \frac{\sin^2\omega_n(g + \cos\omega_n)}{(d + 2g\cos\omega_n)(\gamma^2(d + 2g\cos\omega_n) - \alpha^2(g + \cos\omega_n)^2)} \Bigg] [\gamma\sqrt{d + 2g\cos\omega_n} + \alpha(g + \cos\omega_n)]. \tag{50}$$

Note that setting $m = 0$ reduces $\alpha = \gamma$. Substituting in the equation above, and using the relation $d = g^2 + f + 1$, it becomes identical to the expression in Eq. (17), as expected.

One can again use the same contour method for evaluating the energy density. By comparing with Eq. (17), the functions F_1 and F_2 can be identified as the two terms obtained by removing the second pair of brackets of Eq. (50). The poles (and branch cuts) of these functions can be seen to be the same except that the poles defined by $\omega = \pm i \sinh^{-1}\sqrt{f}$ are now given by

$$\cos(\omega) = y \pm z, \tag{51}$$

where y and z are defined as

$$y = g\left(\frac{\gamma^2}{\alpha^2} - 1\right) \tag{52}$$

$$z = \frac{\gamma}{\alpha}\sqrt{g^2\left(\frac{\gamma^2}{\alpha^2} - 1\right) + f + 1}. \tag{53}$$

As proved in Appendix C, $z - y > 1$, making $\mathrm{abs}(\cos\omega) > 1$ or ω purely imaginary. The pole $\omega = i\cosh^{-1}(y + z)$ lies on the imaginary axis while that for $\omega = i\cosh^{-1}(y - z)$ lies on parallel lines shifted by $\pm\pi$. The choice of contour can be made similar to that in Fig. 8, allowing only the former to contribute to the energy density.

Setting $m = 0$, it is easy to verify that this approach also yields precisely the result in Eq. (A7) by selecting the contour as in the upper half plane of Fig. 8. Its analog for $m \neq 0$ can be obtained by computing the residue at the pole defined by Eq. (51). Instead of giving the full expression again, we only indicate how the results in the continuum limit arise. The pole positions can be computed to be

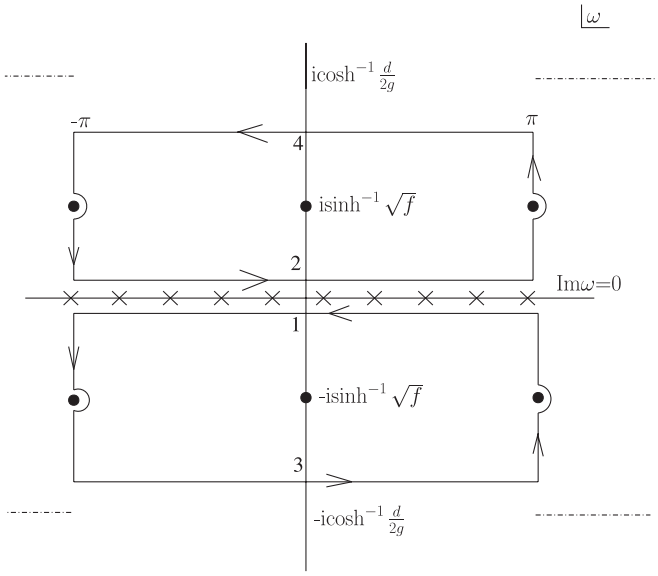

FIG. 8. The choice of contours for evaluating the ω sum in Eq. (17). The dashed lines represent branch cuts. The crosses denote the Matsubara frequencies ω_n, while the filled circles denote the poles of $F(\omega)$.

$$\cos\omega = \alpha_1 = \left(1 + \frac{a^2(\vec{p}^2 + m^2)}{2}\right), \tag{54}$$

and denoting by $m' = m(M-2)/M$

$$\cos\omega = \alpha_2 = -\left(1 + \frac{a^2(\vec{p}^2 + m'^2)}{2}\right), \tag{55}$$

where $\vec{p}^2 = p_1^2 + p_2^2 + p_3^2$. The pole at α_1 has, at order a, the residue

$$\mathrm{Res}\, F_1(\alpha_1) = \pm\frac{a\sqrt{\vec{p}^2 + m^2}}{2}.$$

Note that all the other poles, including the poles at α_2, and the branch cuts do not contribute to the contour integrals, as seen in Fig. 8. Therefore the energy density in the continuum comes out to be the same as in Eq. (20) but with $E = \sqrt{m^2 + p_1^2 + p_2^2 + p_3^2}$.

V. SUMMARY

Investigating the thermodynamics of QCD on lattice with fermions which possess both the chiral symmetry and the flavor symmetry relevant to our world has important consequences for both the experimental aspects of the heavy ion collisions and the theoretical aspects of the $\mu - T$ phase diagram. Staggered fermions used in the bulk of the work so far are not adequate to resolve some of these issues. Overlap fermions, while computationally more expensive, may prove better in such studies in the near future.

We have presented analytical and numerical results on the thermodynamics of free overlap fermions in 4D both for zero and nonzero (baryonic) chemical potential by varying the irrelevant parameter M. From the energy density computed on the lattice in these cases, we showed that the expected continuum limit is reached. Generalizing the proposed action [5] for nonzero μ, we demonstrated that the μ^2 divergence in the continuum limit is avoided for a class of functions $K(\hat{\mu})$ and $L(\hat{\mu})$ with $K(\hat{\mu}) \cdot L(\hat{\mu}) = 1$; the choice $\exp(\pm\hat{\mu})$ for K, L also satisfies this condition and is therefore shown to be free of any μ^2 divergence. In all of these cases, however, the chiral invariance of the action is lost for nonzero μ.

While the signum function in the free overlap Dirac operator remains a constant in computations for $\mu = 0$, we pointed out that it becomes undefined on lattices with odd number of temporal sites for $\mu \geq \mu_c$, where the value of μ_c depends on M. Our numerical computations were restricted to smaller μ values. The numerical results were mildly dependent on the aspect ratio of the spatial and temporal direction but changed significantly as a function of the irrelevant parameter M of the overlap Dirac operator. For the choice of $1.5 \leq M \leq 1.6$, both the energy density and the quark number susceptibility computed for $\mu = 0$ exhibited the smallest deviations from the ideal gas limit, as seen in Fig. 4. As seen from Figs. 1, 6, and 7, lattice results approximate the continuum well for lattices with 12 or more temporal sites, with typically a factor ≈ 1.8 larger results for smaller lattices with 6–8 temporal sites. It would be interesting to check whether the optimum M range is still the same in the presence of gauge fields.

ACKNOWLEDGMENTS

S. S. would like to acknowledge the Council of Scientific and Industrial Research (CSIR) for financial support and thank Saumen Datta for useful discussions.

APPENDIX A: ENERGY DENSITY FOR $\mu = 0$

Before we show the details of the energy density calculation, let us list certain useful relations amongst the quantities g, d, b, and c introduced in Eq. (16), (which will be useful for the calculations below).

(i) Since $\cos(ap_j) \leq 1$ for any j, $g < 0$ for $M < 1$,

(ii) $g^2 + f + 1 = d \Rightarrow d > 0$, since f is a sum of squares,

(iii) $d^2/4g^2 - f - 1 = (g^2 - f - 1)^2/2g^2 \Rightarrow d^2/2g^2 > 1 + f$,

(iv) $\cosh^{-1}\frac{d}{2g} > \sinh^{-1}\sqrt{f}$. This follows trivially from the line above. Since $\frac{d^2}{4g^2} > (1+f)$, it follows $\frac{d}{2g} > \sqrt{1+f}$ ($\frac{d}{2g} < -\sqrt{1+f}$, for $g < 0$). Noting that $\cosh(\sinh^{-1}\sqrt{f}) = \sqrt{1+f}$, one has $\cosh^{-1}(\frac{d}{2g}) > \sinh^{-1}\sqrt{f}$ ($\cosh^{-1}(\frac{d}{2g}) < -\sinh^{-1}\sqrt{f}$ for $g < 0$).

The last line justifies the drawing of the contour in Fig. 8 by avoiding the poles/cuts at $\pm i\cosh^{-1}(\frac{d}{2g})$.

The summation over all Matsubara frequencies $\omega_n = \frac{(2n+1)\pi}{N_T}$ can be done using the standard textbook [18] method of contours in the complex ω plane. For a general function $F(\omega)$ (which in addition may, and does, depend on other variables such as p_j, but this dependence will not be shown explicitly below), the frequency sum therefore is

$$\frac{2\pi}{N_T}\sum_n F(\omega_n) = \int_{\pi-i\epsilon}^{-\pi-i\epsilon} \frac{F(\omega)d\omega}{e^{i\omega N_T}+1} + \int_{-\pi+i\epsilon}^{\pi+i\epsilon} \frac{F(\omega)d\omega}{e^{i\omega N_T}+1}, \tag{A1}$$

where the integrals are evaluated on the contour lines running parallel to the real axis. The second integral can further be rewritten as

$$\int_{-\pi+i\epsilon}^{\pi+i\epsilon} \frac{F(\omega)d\omega}{e^{i\omega N_T}+1} = \int_{-\pi+i\epsilon}^{\pi+i\epsilon} F(\omega)d\omega - \int_{-\pi+i\epsilon}^{\pi+i\epsilon} \frac{F(\omega)d\omega}{e^{-i\omega N_T}+1}. \tag{A2}$$

The summand $F(\omega)$ in Eq. (17) can be split into two terms,

$$F(\omega) = F_1(\omega) + F_2(\omega),$$

with

$$F_1(\omega) = \left(\frac{(1-\cos\omega)}{d+2g\cos\omega} + \frac{\sin^2\omega(g+\cos\omega)}{(d+2g\cos\omega)(f+\sin^2\omega)}\right) \times (g+\cos\omega), \tag{A3}$$

and

$$F_2(\omega) = \left(\frac{(1-\cos\omega)}{d+2g\cos\omega} + \frac{\sin^2\omega(g+\cos\omega)}{(d+2g\cos\omega)(f+\sin^2\omega)}\right) \times \sqrt{d+2g\cos\omega}. \tag{A4}$$

Both the functions F_i have a finite number of poles at $\omega = \pm i\sinh^{-1}\sqrt{f}$ and $\pm m\pi \pm i\sinh^{-1}\sqrt{f}$, where m is an integer. Furthermore, F_1 has poles for $\frac{d}{2g} > 0$ at $\omega = \pm k\pi \pm i\cosh^{-1}\frac{d}{2g}$ while F_2 has branch points at the same locations. Similarly, for $\frac{d}{2g} < 0$ the poles (branch points) of F_1 (F_2) are at $\pm i\cosh^{-1}\frac{d}{2g}$. In the rest of the complex ω plane both the functions are analytic. In view of these properties the contours in Eq. (A1) can be deformed to the contours shown in Fig. 8. We chose each contour such that it lies below (above) the cut in the upper (lower) half of the plane. As shown above, $\cosh^{-1}\frac{d}{2g} > \sinh^{-1}\sqrt{f}$. Defining therefore $2\eta = \cosh^{-1}\frac{d}{2g} - \sinh^{-1}\sqrt{f}$ with $\eta > 0$, the lines 3 and 4 are drawn through the points $\mp(i\sinh^{-1}\sqrt{f} + i\eta)$ respectively to avoid the cuts shown in Fig. 8.

Consequently, the frequency sum in Eq. (A1) becomes

$$\frac{2\pi}{N_T}\sum_n F(\omega_n) = -2\pi i \sum_{\mathrm{Im}\omega>0} \frac{\mathrm{Res}F(\omega)}{e^{-i\omega N_T}+1} + 2\pi i \sum_{\mathrm{Im}\omega<0} \frac{\mathrm{Res}F(\omega)}{e^{i\omega N_T}+1} - \int_3 \frac{F(\omega)d\omega}{e^{i\omega N_T}+1} + \int_4 \frac{F(\omega)d\omega}{e^{-i\omega N_T}+1} + \int_{-\pi+i\epsilon}^{\pi+i\epsilon} F(\omega)d\omega. \tag{A5}$$

Note that the line integrals along the vertical lines through π and $-\pi$ cancel each other due to the periodicity of the function $F(\omega)$. Indeed, in general for any function $G(\omega)$ satisfying the property $G(\pi+i\eta) = G(-\pi+i\eta)$, the sum of integrals of $G(\omega)$ along opposite vertical paths of equal length through $-\pi$ and π is identically zero.

The residues of the function $F_{1,2}(\omega)$ at the poles $\omega = \pm i\sinh^{-1}\sqrt{f}$ are $\pm iR_1$ and $\pm iR_2$ respectively where

$$R_1 = R_2 = \frac{\sqrt{f}}{2\sqrt{1+f}}. \tag{A6}$$

Our choice of the contour ensures that the poles at $\pm\pi \pm i\sinh^{-1}\sqrt{f}$ do not contribute to the energy density. By taking the limit $N_T \to \infty$ on the lattice, one finds that the last term of Eq. (A5) gives the quartically divergent vacuum contribution in the continuum limit. Defining the physical energy density by subtracting it off, we have

$$\epsilon a^4 = \frac{4}{N^3}\sum_{p_j}\left[\frac{\sqrt{f}}{\sqrt{1+f}}\right]\frac{1}{e^{N_T\sinh^{-1}\sqrt{f}}+1} + \epsilon_3 + \epsilon_4, \tag{A7}$$

where ϵ_3, ϵ_4 terms come from the line integrals 3 and 4, respectively.

APPENDIX B: ENERGY DENSITY AT $T \neq 0$ AND $\mu \neq 0$

For evaluating the energy density, we revert back to the choice $K(\hat{\mu}) = \exp(\hat{\mu})$ and $L(\hat{\mu}) = \exp(-\hat{\mu})$ which has $R = 1$ and $\theta = \hat{\mu}$. The physical part of the energy density on the lattice is calculated by subtracting off the $\hat{\mu} = 0$, $T = 0$ contribution,

$$\epsilon a^4 = \sum_{p_j}\frac{1}{N^3}\left[\frac{2}{N_T}\sum_n F(\omega_n - i\hat{\mu}) - \frac{1}{\pi}\int_{-\pi}^{\pi} F(\omega)d\omega\right]. \tag{B1}$$

The further evaluation of the energy density can be done, noting that, compared to Fig. 8, the Matsubara frequencies $(2n+1)\pi/N_T$ in this case are displaced along the imaginary axis by $i\hat{\mu}$ in the lower half plane with the choice of the function $1/(\exp[i(\omega + i\hat{\mu})N_T] + 1)$. The frequency sum can be replaced by line integrals as

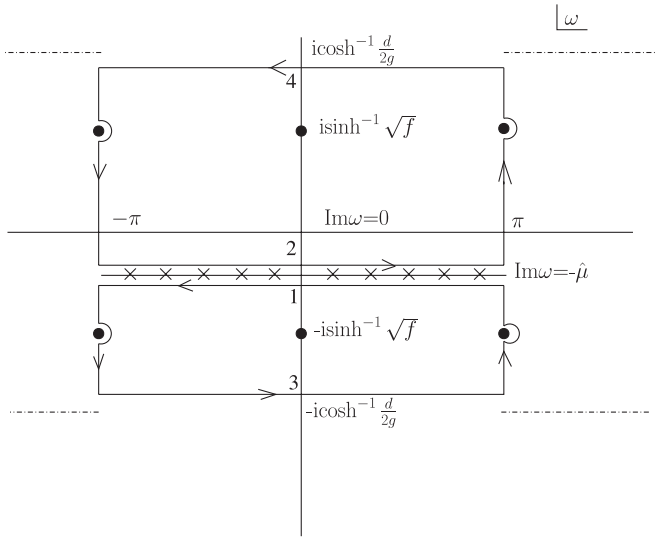

FIG. 9. The contours chosen for evaluation of the ω sum for $\hat{\mu} < \sinh^{-1}\sqrt{f}$. Same notation as in Fig. 8.

$$\frac{2\pi}{N_T}\sum_n F(\omega_n - i\hat{\mu}) = \int_{\pi - i\epsilon - i\hat{\mu}}^{-\pi - i\epsilon - i\hat{\mu}} \frac{F(\omega)d\omega}{e^{i(\omega+i\hat{\mu})N_T}+1} + \int_{-\pi+i\epsilon-i\hat{\mu}}^{\pi+i\epsilon-i\hat{\mu}} \frac{F(\omega)d\omega}{e^{i(\omega+i\hat{\mu})N_T}+1}. \tag{B2}$$

The choice of the contour will be analogous to that in Fig. 8, but will depend on whether the pole $\omega = -i\sinh^{-1}\sqrt{f}$ is above or below the Im$\omega = -\hat{\mu}$ line. Therefore the frequency sum can be split into two terms,

$$\sum_n F(\omega_n - i\hat{\mu}) = \sum_n [F_<(\omega_n - i\hat{\mu}) + F_>(\omega_n - i\hat{\mu})], \tag{B3}$$

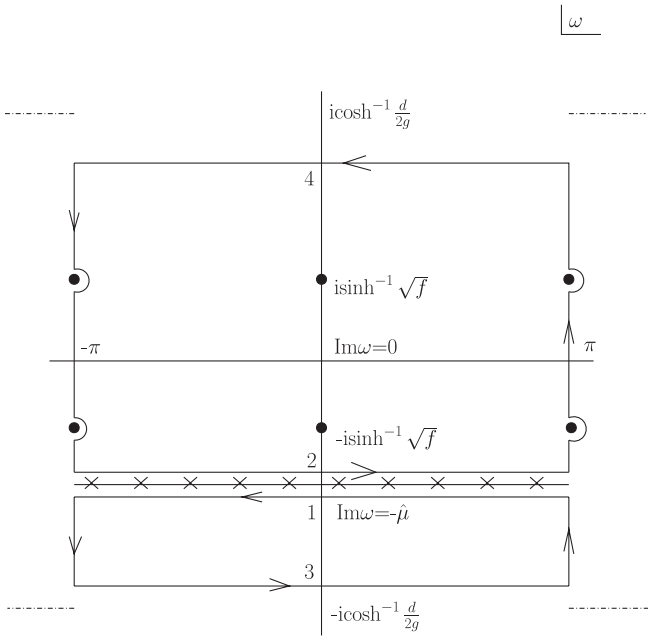

FIG. 10. The contours chosen for evaluation of the ω sum for $\hat{\mu} > \sinh^{-1}\sqrt{f}$. Same notation as in Fig. 8.

where $F_>$ and $F_<$ are the functions with $\sinh^{-1}\sqrt{f} < \hat{\mu}$ and $\sinh^{-1}\sqrt{f} > \hat{\mu}$, respectively. We have taken $\hat{\mu} < \cosh^{-1}\frac{d}{2g}$ because we expect that in the continuum limit the $\hat{\mu}$ will scale as the lattice spacing whereas the second term will tend to infinity. For the case $\hat{\mu} < \sinh^{-1}\sqrt{f}$, the contour was chosen as shown in Fig. 9.

Using the standard trick of rewriting the second integral in Eq. (B2) as done in Eq. (A2) the frequency sum becomes

$$\frac{2\pi}{N_T}\sum_n F_<(\omega_n - i\hat{\mu}) = \Theta(\sinh^{-1}\sqrt{f} - \hat{\mu})\Big(-2\pi i \sum_{\mathrm{Im}\omega>0} \frac{\mathrm{Res}F(\omega)}{e^{-i(\omega+i\hat{\mu})N_T}+1} + 2\pi i \sum_{\mathrm{Im}\omega<0} \frac{\mathrm{Res}F(\omega)}{e^{i(\omega+i\hat{\mu})N_T}+1} - \int_3 \frac{F(\omega)}{e^{i(\omega+i\hat{\mu})N_T}+1}d\omega + \int_4 \frac{F(\omega)}{e^{-i(\omega+i\hat{\mu})N_T}+1}d\omega + \int_{-\pi}^{\pi} F(\omega)d\omega\Big). \tag{B4}$$

The expression can be evaluated by substituting the values of the residues of the function $F(\omega)$, which are the sum of residues calculated in Eq. (A6). The integrals 3 and 4 are along the lines Im$\omega = \mp(\sinh^{-1}\sqrt{f} + \eta)$. Representing them as $\epsilon_{3\mu,4\mu}$ respectively, we get

$$\frac{2\pi}{N_T}\sum_n F_<(\omega_n - i\hat{\mu}) = \Theta(\sinh^{-1}\sqrt{f} - \hat{\mu})\Big(\frac{4\pi R_1}{e^{(\sinh^{-1}\sqrt{f}+\hat{\mu})N_T}+1} + \frac{4\pi R_1}{e^{(\sinh^{-1}\sqrt{f}-\hat{\mu})N_T}+1} + \int_{-\pi}^{\pi} F(\omega)d\omega + \epsilon_{3\mu} + \epsilon_{4\mu}\Big). \tag{B5}$$

Similarly for $\hat{\mu} > \sinh^{-1}\sqrt{f}$ the frequency sum is replaced by integrals along the contour as shown in Fig. 10. There are no poles below the Im$\omega = -\hat{\mu}$ line so the first integral in Eq. (B2) can be replaced by a line integral along the line 3. Following the same steps as discussed for the above case, the frequency sum reduces to

$$\frac{2\pi}{N_T}\sum_n F_>(\omega_n - i\hat{\mu}) = \Theta(\hat{\mu} - \sinh^{-1}\sqrt{f})\left(\frac{4\pi R_1}{e^{(\sinh^{-1}\sqrt{f}-\hat{\mu})N_T}+1} + \frac{4\pi R_1}{e^{(\sinh^{-1}\sqrt{f}+\hat{\mu})N_T}+1} + \int_{-\pi}^{\pi} F(\omega)d\omega + \epsilon_{3\mu} + \epsilon_{4\mu}\right). \tag{B6}$$

Finally, the energy density on the lattice is obtained from Eq. (B1) by substituting in Eq. (B3) the frequency sums calculated above,

$$\epsilon a^4 = \frac{2}{N^3}\sum_{p_j}\left[\frac{\sqrt{f}}{\sqrt{1+f}}\frac{1}{e^{(\sinh^{-1}\sqrt{f}-\hat{\mu})N_T}+1} + \frac{\sqrt{f}}{\sqrt{1+f}}\frac{1}{e^{(\sinh^{-1}\sqrt{f}+\hat{\mu})N_T}+1} + \epsilon_{3\mu} + \epsilon_{4\mu}\right]. \tag{B7}$$

APPENDIX C

Here we prove the claim made in Eq. (51).

(i) $y > 0$ since $\gamma > \alpha$.

(ii) Let $\xi = \frac{\gamma^2}{\alpha^2} - 1$, where $\xi > 0$.

(iii) A little algebra shows that $z^2 - (y+1)^2 = \xi[(g-1)^2 + f] + f > 0$ which in turn implies the relation $z - y > 1$.

[1] F. Karsch, E. Laermann, and A. Peikert, Phys. Lett. B **478**, 447 (2000).
[2] E. Laermann and O. Philipsen, Annu. Rev. Nucl. Part. Sci. **53**, 163 (2003).
[3] K. Rajagopal and F. Wilczek, in At the Frontier of Particle Physics/Handbook of QCD, edited by M. Shifman (World Scientific, Singapore, 2001), Vol. 3, p. 2061.
[4] R. Narayanan and H. Neuberger, Phys. Rev. Lett. **71**, 3251 (1993); H. Neuberger, Phys. Lett. B **417**, 141 (1998).
[5] J. Bloch and T. Wettig, Phys. Rev. Lett. **97**, 012003 (2006).
[6] C. Gattringer and L. Liptak, Phys. Rev. D **76**, 054502 (2007).
[7] R. V. Gavai, Phys. Rev. D **32**, 519 (1985).
[8] P. H. Ginsparg and K. G. Wilson, Phys. Rev. D **25**, 2649 (1982).
[9] M. Luscher, Phys. Lett. B **428**, 342 (1998).
[10] W. Bietenholz, Eur. Phys. J. C **6**, 537 (1999).
[11] P. Hegde *et al.*, Eur. Phys. J. C **55**, 423 (2008).
[12] W. Bietenholz *et al.*, Nucl. Phys. B, Proc. Suppl. **53**, 921 (1997); W. Bietenholz and U. J. Wiese, Phys. Lett. B **426**, 114 (1998).
[13] W. Bietenholz and I. Hip, Nucl. Phys. **B570**, 423 (2000).
[14] Y. Kikukawa and A. Yamada, arXiv:hep-lat/9810024; P. Hasenfratz *et al.*, Nucl. Phys. **B643**, 280 (2002).
[15] J. E. Mandula, arXiv:0712.0651.
[16] P. Hasenfratz and F. Karsch, Phys. Lett. **125B**, 308 (1983).
[17] N. Bilic and Rajiv V. Gavai, Z. Phys. C **23**, 77 (1984).
[18] H. J. Rothe, *Lattice Gauge Theories: An Introduction* (World Scientific, Singapore, 1998), 2nd ed..